processes

MDPI

Article

Anticipation Augment-Assisted Active Disturbance Rejection Control and Its Application in SCR Denitrification Systems

Jianbo Liu [1], Jiacheng Peng [1], Jingjing Wang [1], Zhiwei Wang [2] and Xiangyang Li [2,*]

[1] Guoneng Guohua (Beijing) Gas-Fired Co., Ltd., Beijing 100018, China; 16100372@ceic.com (J.L.); 16051818@ceic.com (J.P.); 16032733@ceic.com (J.W.)
[2] School of Automation Science and Engineering, South China University of Technology, Guangzhou 510641, China; tian1344@outlook.com
* Correspondence: xyangli@scut.edu.cn

Abstract

Selective catalytic reduction (SCR) denitrification systems in coal-fired power plants exhibit large inertia, pronounced dynamic lag, time-varying parameters, catalyst ammonia-storage effects, and multiple disturbances, which limit the control performance of outlet nitrogen oxides (NOx). To address these issues, an anticipation augment-assisted active disturbance rejection control (AA-ADRC) framework is proposed and implemented in a linear form. The dynamic characteristics of classical mechanistic, improved mechanistic, and existing industrially identified SCR models are first analyzed, and a control-oriented linear active disturbance rejection control (LADRC) model is established based on the identified second-order ammonia-injection control channel. A finite-bandwidth filtered-derivative component is then extracted from the ammonia-injection command and converted into a finite-bandwidth anticipatory process increment. The augmented signal is introduced into the extended state observer (ESO), allowing input-variation information to participate earlier in state estimation and disturbance compensation while retaining the estimation and compensation of the generalized disturbance. Comparative simulations with proportional–integral (PI) and LADRC under inlet NOx step disturbances, composite inlet NOx disturbances, outlet NOx disturbances, and ammonia-injection disturbances show that AA-ADRC provides faster transient recovery in the step-disturbance case and reduces ammonia-command variation.

Keywords: selective catalytic reduction; active disturbance rejection control (ADRC); an anticipation augment-assisted active disturbance rejection control (AA-ADRC); extended state observer (ESO); disturbance rejection

Check for updates

Academic Editor: Giampaolo Manzolini

Received: 23 August 2026
Revised: 17 October 2026
Accepted: 20 October 2026
Published: 23 October 2026

Copyright: © 2026 by the authors. Licensee MDPI, Basel, Switzerland. This article is an open access article distributed under the terms and conditions of the Creative Commons Attribution (CC BY) license.

1. Introduction

Nitrogen oxides (NOx) are among the major atmospheric pollutants emitted by coal-fired power plants. Their emissions contribute to acid rain, photochemical pollution, ecological degradation, and adverse human-health effects [1,2]. Selective catalytic reduction (SCR) has become the principal technology for controlling NOx emissions from large coal-fired generating units because of its high denitrification efficiency and technological maturity [3,4]. In a typical SCR process, ammonia (NH_3) is injected as the reducing agent to convert NOx into nitrogen and water over the catalyst [5]. Insufficient ammonia injection leads to excessive outlet NOx emissions, whereas excessive injection increases ammonia slip and may cause air-preheater blockage, corrosion, and additional operating costs [6,7]. Maintaining the outlet NOx concentration within the emission limit while avoiding unnecessary ammonia consumption is therefore a central control objective of SCR systems [8,9].

Coal-fired generating units increasingly operate under deep peak regulation—i.e., at substantially reduced load levels to accommodate power-system demand fluctuations and renewable-energy integration—and under frequent load-following conditions, making SCR control more challenging [10]. Load variations simultaneously change the inlet NOx concentration, flue-gas flow rate, flue-gas temperature, and catalyst operating conditions [11,12]. The effect of ammonia injection must also propagate through dilution, mixing, species transport, adsorption, internal diffusion, and catalytic reactions before it becomes visible in the outlet NOx concentration [13,14]. Ammonia storage and release within the catalyst further introduce dynamic memory into the process [15]. Consequently, the ammonia-injection control channel exhibits large inertia, pronounced phase lag, time-varying characteristics, and uncertain internal dynamics. These properties create a substantial mismatch between the ammonia-injection command and the measured outlet response.

Proportional–Integral–Derivative (PID) control and its modified structures remain widely used in industrial processes because of their simple architecture and convenient implementation [9,16]. Their performance, however, depends strongly on the operating condition used for parameter tuning. Changes in unit load, inlet NOx concentration, and catalyst activity may alter the process gain and time constants, resulting in sluggish response, overshoot, or excessive ammonia-injection fluctuations [10,17]. Feedforward control, gain scheduling, and intelligent ammonia-injection strategies have also been investigated [18,19], but they generally rely on reliable measurements, operating-region partitioning, or extensive empirical knowledge, with limited capability for handling unmodeled dynamics and multiple simultaneous disturbances.

Model predictive control (MPC) provides a systematic framework for handling multivariable interactions, actuator constraints, and performance optimization [20,21]. In SCR applications, MPC predicts the future outlet NOx response and optimizes the ammonia-injection command over a receding horizon [9,17]. Its performance, however, depends strongly on prediction-model accuracy. Detailed mechanistic models involve numerous kinetic parameters and unmeasurable states, whereas low-order data-driven models may lose accuracy with catalyst aging or operating-range changes [11,22]. The associated online optimization and model maintenance may also limit industrial implementation.

ADRC provides an alternative approach for systems with uncertain dynamics. It employs an ESO to estimate the combined influence of internal dynamics, parameter variations, unmodeled characteristics, and external disturbances as a generalized disturbance [23,24]. The estimated disturbance is then compensated in real time. The convergence and disturbance-estimation properties of the ESO have been extensively investigated [25,26]. Compared with strongly model-dependent methods, ADRC mainly requires knowledge of the dominant relative degree and an approximate control-gain magnitude, which makes it attractive for industrial processes with uncertain parameters [27]. For SCR systems, catalyst-storage dynamics, reaction uncertainties, inlet variations, and operating-condition changes can be incorporated into the generalized disturbance, reducing direct dependence on detailed kinetic parameters.

Conventional ADRC mainly corrects its state and disturbance estimates through the current output-measurement error [23,25], while the known control input, although already incorporated into the LESO through the nominal input channel, mainly represents the direct control action in the observer model, and its transient variation is not explicitly utilized in the measurement process. After the ammonia-injection command changes, its effect must propagate through the slow process dynamics before becoming sufficiently pronounced in the outlet NOx measurement. Increasing the controller or observer bandwidth cannot eliminate this physical propagation lag [28,29]. Excessive bandwidth may instead amplify measurement fluctuations, produce abrupt ammonia-injection commands, and increase the

risk of actuator saturation [27,30]. Earlier utilization of the transient variation information of the ammonia-injection input is therefore desirable to improve the dynamic response without sacrificing the disturbance-estimation capability of ADRC.

The objective of this study is to improve outlet-NOx regulation and reduce excessive ammonia-command variation in SCR systems with large inertia, slow response, and multiple disturbances. A control-oriented model is first established from the identified second-order ammonia-injection control channel, with LADRC adopted as the specific control realization. On this basis, an anticipation augment-assisted linear active disturbance rejection control (AA-LADRC) is developed by introducing a finite-bandwidth anticipatory process increment derived from the ammonia-injection command into the ESO. Compared with anticipatory NH_3-injection control based on inlet-NOx prediction [19], predictive or modified ADRC methods for time-delay systems [28,29], and phase-compensation-based ADRC for high-order, large-inertia processes [31], AA-LADRC neither predicts future NOx trajectories nor introduces additional delay- or phase-compensation structures. Instead, it exploits the transient variation in the known ammonia-injection command to reshape the LESO measurement channel. The identified SCR model and basic LADRC structure are adopted from existing studies, while the anticipation augment path and the corresponding boundedness analysis constitute the main contributions of this work.

The remainder of this paper is organized as follows. Section 2 introduces the SCR process and analyzes the dynamic characteristics of different models. Section 3 develops the proposed AA-LADRC structure, and Section 4 presents its stability analysis. Section 5 describes parameter tuning and comparative simulations under inlet NOx variations and multiple disturbances. Section 6 concludes the paper.

2. SCR Denitrification System and Reaction Mechanism

2.1. Mechanism-Based Modeling of the SCR Denitrification Process

In the SCR process, NH_3 is vaporized, diluted with air, injected into the flue-gas duct through an ammonia injection grid, and mixed with the NOx-containing flue gas before passing through the catalyst layers. The principal reactions include the standard SCR reaction, the NO2-SCR reaction, and the fast SCR reaction [4,5,32,33], whose stoichiometric relationships are expressed as

$$\begin{aligned} &4NO + 4NH_3 + O_2 \rightarrow 4N_2 + 6H_2O, \\ &2NO_2 + 4NH_3 + O_2 \rightarrow 3N_2 + 6H_2O, \\ &NO + NO_2 + 2NH_3 \rightarrow 2N_2 + 3H_2O. \end{aligned} \tag{1}$$

The SCR denitrification efficiency is jointly affected by the inlet NOx concentration, flue-gas temperature, flue-gas flow rate, catalyst activity, and the spatial uniformity of the NH_3/NOx distribution. Insufficient ammonia injection results in incomplete NOx reduction, whereas excessive ammonia injection increases ammonia slip and may adversely affect the safe and stable operation of downstream equipment.

Most SCR kinetic models are formulated according to the Eley–Rideal mechanism, in which adsorbed ammonia reacts with gaseous or weakly adsorbed NO on the catalyst surface [3,13–15,34,35]. On this basis, the main kinetic processes can be described by

$$\begin{aligned} r_a &= k_a^0 \exp\left(-\tfrac{E_a}{RT}\right) C_{NH_3}(1-\theta_{NH_3}), \\ r_d &= k_d^0 \exp\left[-\tfrac{E_d(1-\alpha\theta_{NH_3})}{RT}\right]\theta_{NH_3}, \\ r_{NO} &= k_{NO}^0 \exp\left(-\tfrac{E_{NO}}{RT}\right) C_{NO}\theta_{NH_3}^*\left[1-\exp\left(-\tfrac{\theta_{NH_3}}{\theta_{NH_3}^*}\right)\right], \\ r_{ox} &= k_{ox}^0 \exp\left(-\tfrac{E_{ox}}{RT}\right)\theta_{NH_3}. \end{aligned} \tag{2}$$

According to the mass-conservation relationships between the gas-phase species and the adsorbed ammonia on the catalyst surface, the classical kinetic model is expressed as

$$\begin{aligned} \frac{\mathrm{d}C_{\mathrm{NH_3}}}{\mathrm{d}t} &= \Omega(r_d - r_a), \\ \frac{\mathrm{d}\theta_{\mathrm{NH_3}}}{\mathrm{d}t} &= r_a - r_d - r_{\mathrm{NO}} - r_{\mathrm{ox}}, \\ \frac{\mathrm{d}C_{\mathrm{NO}}}{\mathrm{d}t} &= -\Omega r_{\mathrm{NO}}. \end{aligned} \tag{3}$$

Here, r_a, r_d, r_{NO}, and r_{ox} denote the ammonia adsorption rate, ammonia desorption rate, NO reduction rate, and oxidation rate of adsorbed ammonia, respectively. The parameters k_a^0, k_d^0, k_{NO}^0, and k_{ox}^0 are the corresponding pre-exponential factors, whereas E_a, E_d, E_{NO}, and E_{ox} are the activation energies. Moreover, C_{NH_3} and C_{NO} denote the gas-phase concentrations of NH_3 and NO, respectively; θ_{NH_3} is the surface coverage of adsorbed ammonia; $\theta^*_{NH_3}$ is the characteristic reaction coverage; α is the coverage-dependent measurement coefficient for the desorption activation energy; R is the universal gas constant; T is the absolute flue-gas temperature; and Ω denotes the equivalent ammonia-storage capacity of the catalyst.

The classical kinetic model was mainly developed using powdered catalyst samples and employs a single coverage state to represent the catalyst ammonia-storage condition. Commercial coal-fired power plants, however, generally use honeycomb or plate-type catalysts with finite wall thickness. Their specific surface area, porous structure, and mass-transfer characteristics differ substantially from those of powdered catalysts. Furthermore, long-term operation leads to ash deposition and pore blockage, thereby restricting the diffusion of NO toward active sites inside the catalyst. In contrast, NH_3 may gradually migrate into the catalyst through desorption, intraporous diffusion, and re-adsorption, and may consequently be stored at internal active sites that are not readily accessible to gaseous NO.

To address this limitation, Rao et al. [36] divided the catalyst ammonia-storage state into surface-adsorbed and internally adsorbed ammonia states and introduced bidirectional mass exchange between the two states. A plug-flow assumption was further employed to describe gas-phase species transport along the axial direction of the reactor. The adsorption, desorption, and NO reduction rates in the improved model are expressed as

$$\begin{aligned} r_a &= k_a^0 \exp\left(-\frac{E_a}{RT}\right) C_{\mathrm{NH_3}} \left(1 - \theta^{\mathrm{surf}}_{\mathrm{NH_3}}\right), \\ r_d &= k_d^0 \exp\left[-\frac{E_d\left(1-\alpha\theta^{\mathrm{surf}}_{\mathrm{NH_3}}\right)}{RT}\right] \theta^{\mathrm{surf}}_{\mathrm{NH_3}}, \\ r_{\mathrm{NO}} &= k_{\mathrm{NO}}^0 \exp\left(-\frac{E_{\mathrm{NO}}}{RT}\right) C_{\mathrm{NO}} \theta^*_{\mathrm{NH_3}} \left[1 - \exp\left(-\frac{\theta^{\mathrm{surf}}_{\mathrm{NH_3}}}{\theta^*_{\mathrm{NH_3}}}\right)\right]. \end{aligned} \tag{4}$$

The migration rates between the internal and surface ammonia-storage states are defined as

$$\begin{aligned} r_{i-s} &= k_{si}^0 \exp\left(-\frac{E_{si}}{RT}\right) \theta^{\mathrm{inter}}_{\mathrm{NH_3}} \left(1 - \theta^{\mathrm{surf}}_{\mathrm{NH_3}}\right), \\ r_{s-i} &= k_{si}^0 \exp\left(-\frac{E_{si}}{RT}\right) \theta^{\mathrm{surf}}_{\mathrm{NH_3}} \left(1 - \theta^{\mathrm{inter}}_{\mathrm{NH_3}}\right). \end{aligned} \tag{5}$$

Under the plug-flow assumption, the gas-phase and ammonia-storage dynamics are governed by

$$\begin{aligned} \frac{\partial C_{\mathrm{NH_3}}}{\partial z} &= \Omega_{\mathrm{surf}} (r_d - r_a) \frac{V_{\mathrm{SCR}}}{Q}, \\ \frac{\partial C_{\mathrm{NO}}}{\partial z} &= -\Omega_{\mathrm{surf}} r_{\mathrm{NO}} \frac{V_{\mathrm{SCR}}}{Q}, \\ \frac{\partial \theta^{\mathrm{surf}}_{\mathrm{NH_3}}}{\partial t} &= r_a - r_d - r_{\mathrm{NO}} + r_{i-s} - r_{s-i}, \\ \frac{\partial \theta^{\mathrm{inter}}_{\mathrm{NH_3}}}{\partial t} &= \frac{\Omega_{\mathrm{surf}}}{\Omega_{\mathrm{inter}}} (r_{s-i} - r_{i-s}). \end{aligned} \tag{6}$$

In (4)–(6), θ^{surf}_{NH3} and θ^{inter}_{NH3} denote the surface and internal ammonia coverages, respectively. The variables r_{i-s} and r_{s-i} denote the ammonia migration rates from the internal

region to the surface and from the surface to the internal region, respectively. Ω_{surf} and Ω_{inter} are the maximum surface and internal ammonia-storage capacities. In addition, V_{SCR} and Q denote the effective flow volume of the SCR reactor and the volumetric flue-gas flow rate, respectively. The variable z denotes the dimensionless normalized axial coordinate along the flue-gas flow direction, defined as $z = H/L \in [0,1]$, where H is the physical axial distance measured from the inlet of the modeled reaction region, and L is the total axial length of that region, both in meters. Because oxidation of adsorbed ammonia is relatively weak within the typical operating-temperature range of coal-fired SCR systems, a separate ammonia-oxidation equation is commonly omitted from the improved model.

The improved model was validated using operating data from the SCR system of a 660 MW coal-fired generating unit equipped with a V_2O_5–WO_3/TiO_2 honeycomb catalyst. The improved model exhibited closer agreement with the measured outlet NOx concentration, smaller local prediction errors, and a limited difference between the training and validation errors. Compared with the classical single-coverage model, the improved model therefore provides better prediction accuracy and generalization capability.

2.2. Industrial Operating Data-Based SCR Identification Modeling

Although mechanistic models provide physical insight into ammonia adsorption, desorption, catalytic reduction, and internal catalyst storage, their online application requires numerous kinetic parameters and unmeasurable internal states. Their complexity also increases considerably with the spatial discretization resolution. To obtain a compact model that captures the overall industrial SCR dynamics, Zeng et al. introduced an identification approach based on converted ammonia flow using closed-loop operating data [17]. By normalizing the actual ammonia flow according to the unit load, the approach reduces the operating-point nonlinearity associated with variations in flue-gas flow and transforms the SCR process into a quasi-linear input–output system.

Neglecting ammonia slip, the mass-conservation relationship of the SCR system can be simplified as

$$c_1 - \frac{1}{r}\frac{m}{G} = c_2 \tag{7}$$

where G denotes the flue-gas flow rate; m is the actual ammonia injection flow; and c_1 and c_2 denote the inlet and outlet NOx concentrations, respectively. The coefficient r accounts for the ammonia-to-NOx reaction mass ratio (the mass of liquid ammonia required to react with a unit mass of NOx) and mass unit conversion.

Equation (7) indicates that the outlet NOx concentration depends not only on the total ammonia injection flow but also on the ammonia injection level per unit flue-gas flow. Therefore, directly using the actual ammonia flow as the model input causes the model dynamics to vary with the operating condition during load changes.

Considering that the flue-gas flow is approximately proportional to the unit load, the converted ammonia flow is introduced as

$$m_P = \frac{m}{N/N_E} = \frac{mN_E}{N} \tag{8}$$

where N and N_E denote the actual and rated unit loads, respectively.

The converted ammonia flow represents the ammonia injection level per unit load and reduces the influence of load variation on the model input. Consequently, the relationship among the inlet NOx concentration, ammonia injection level, and outlet NOx concentration can be regarded as approximately linear within a specified operating range.

Based on the above treatment, a dual-input single-output dynamic model was established as

$$Y(s) = G_u(s)U(s) + G_d(s)D(s), \tag{9}$$

where $Y(s)$ denotes the absolute outlet NOx concentration, $U(s)$ denotes the absolute converted ammonia-flow input, and $D(s)$ denotes the absolute inlet NOx concentration. Moreover, $Gu(s)$ and $Gd(s)$ represent the dynamic transfer characteristics of the ammonia-injection control channel and the inlet disturbance channel, respectively.

The identification data were obtained from one flue-gas branch of the SCR system in a 300 MW coal-fired generating unit. The measured variables included the actual unit load, inlet NOx concentration, actual ammonia flow, and outlet NOx concentration. Approximately 100,000 s of operating data were used for model identification, and an additional 50,000 s for validation, with a sampling interval of 5 s. Using the converted ammonia flow, the mean absolute deviations were 2.787 and 2.931 mg/Nm^3 for identification and validation, respectively, compared with 4.450 and 4.529 mg/Nm^3 when the actual ammonia flow was used directly. The identified transfer functions contain no explicit pure transport-delay term; the slow SCR response is instead represented by the relatively large time constants of the low-order dynamics.

2.3. Comparison of SCR Modeling Approaches

Different SCR modeling approaches exhibit significant differences in model complexity, physical interpretability, and suitability for control applications. Mechanistic models provide strong physical insights; however, their high parameter dependence and the difficulty in obtaining internal states online limit their direct application in real-time control. Although improved mechanistic models further consider ammonia-storage dynamics and mass-transfer processes, they also introduce higher model orders and increased computational burdens. In contrast, industrial data-identified models directly establish dynamic relationships using measurable operating variables, featuring simpler structures, higher computational efficiency, and better applicability for online implementation. Therefore, for real-time SCR control, an appropriate model should balance the capability of describing the dominant dynamic characteristics with model simplicity and computational efficiency.

3. Control-Oriented Modeling and AA-LADRC for SCR Systems

3.1. LADRC Representation of the Industrially Identified Model

The SCR model identified from industrial operating data consists of a second-order ammonia-injection control channel and a first-order inlet NOx disturbance channel:

$$G_u(s) = \frac{K_u}{(T_1 s + 1)(T_2 s + 1)}, \quad G_d(s) = \frac{K_d}{T_d s + 1}. \tag{10}$$

Here, u is the converted ammonia flow, d is the inlet NOx concentration, and y is the outlet NOx concentration. By representing the combined effect of the inlet NOx disturbance and unmodeled dynamics as $q(t)$, the control-oriented time-domain model is written as

$$\ddot{y} = -\frac{T_1 + T_2}{T_1 T_2}\dot{y} - \frac{1}{T_1 T_2} y + b_i u + \frac{q(t)}{T_1 T_2}, \quad b_i = \frac{K_u}{T_1 T_2} < 0 \tag{11}$$

Introducing a constant nominal control gain, b_{i0}, with the same sign as b_i, the identified model is transformed into the LADRC canonical form.

$$\begin{aligned} \ddot{y} &= f_i + b_{i0} u \\ f_i &= -\tfrac{T_1+T_2}{T_1 T_2}\dot{y} - \tfrac{1}{T_1 T_2} y + \tfrac{q(t)}{T_1 T_2} + (b_i - b_{i0}) u \end{aligned} \tag{12}$$

The generalized disturbance, f_i, incorporates the nominal plant dynamics, inlet NOx disturbances, parameter variations, unmodeled dynamics, and control-gain mismatch.

Since the identified ammonia-injection control channel has a relative degree of two, a third-order linear extended-state observer (LESO) is constructed as

$$\begin{cases} \dot{z}_1 = z_2 + \beta_1(y - z_1), \\ \dot{z}_2 = z_3 + b_{i0}u + \beta_2(y - z_1), \\ \dot{z}_3 = \beta_3(y - z_1). \end{cases} \tag{13}$$

where z_1, z_2, and z_3 estimate y, $\dot{y}$, and f_i, respectively.

The corresponding LADRC law is

$$u = \frac{v - z_3}{b_{i0}}, \quad v = k_p(y_{ref} - z_1) - k_v z_2 \tag{14}$$

where y_{ref} denotes the outlet NOx reference, and k_p and k_v are the controller gains.

The industrially identified model is selected as the nominal plant for the subsequent LADRC design, while the mechanistic models are retained to interpret the physical origins and composition of the generalized disturbance. The resulting LADRC control structure for the SCR denitrification system is shown in Figure 1.

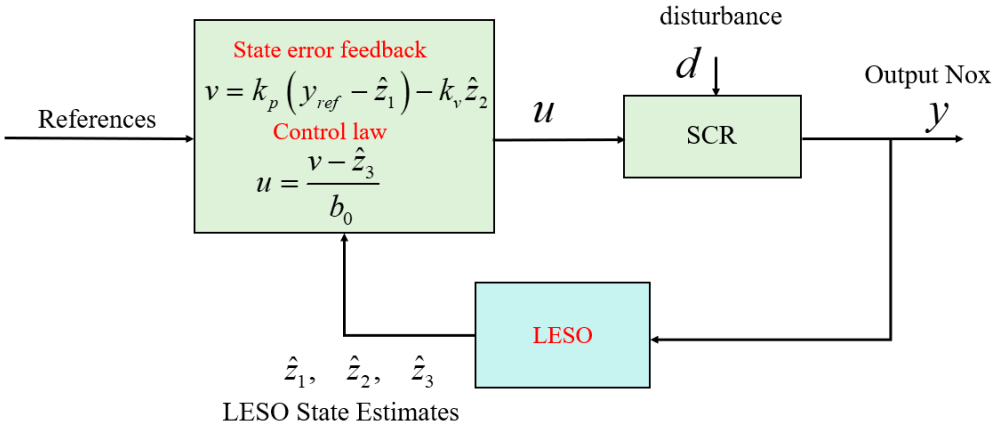


Figure 1. Control structure of LADRC for SCR denitrification.

Nevertheless, the identified ammonia-injection control channel still contains two large time constants. The resulting dynamic lag limits the transient performance of conventional LADRC. Although the LESO can estimate model mismatch and external disturbances, its measurement is mainly generated after the ammonia-injection effect becomes visible in the outlet NOx measurement. Directly increasing the controller or observer bandwidth may amplify measurement noise and cause excessive variations in the ammonia-injection command.

3.2. Design of AA-LADRC via Filtered-Derivative Anticipation Augment

For the SCR process with pronounced inertia and dynamic lag, variations in the ammonia-injection command generally precede the measurable response of the outlet NOx concentration. Although the outlet NOx measurement may not exhibit an immediate change, the transient variation in the ammonia-injection command provides input-side dynamic information before the corresponding output variation becomes sufficiently measurable. This information can therefore be used to construct a corresponding anticipation augment, allowing it to participate in observer measurement before the actual outlet response becomes sufficiently pronounced.

Based on this characteristic, a finite-bandwidth filtered-derivative component is extracted from the ammonia-injection input and converted into an anticipation augment using the transient input-side information. The augmented measurement is then supplied to the LESO, allowing the transient input-side information to participate in observer measurement

before the corresponding variation becomes sufficiently pronounced in the actual outlet measurement. The resulting AA-LADRC control structure is shown in Figure 2.

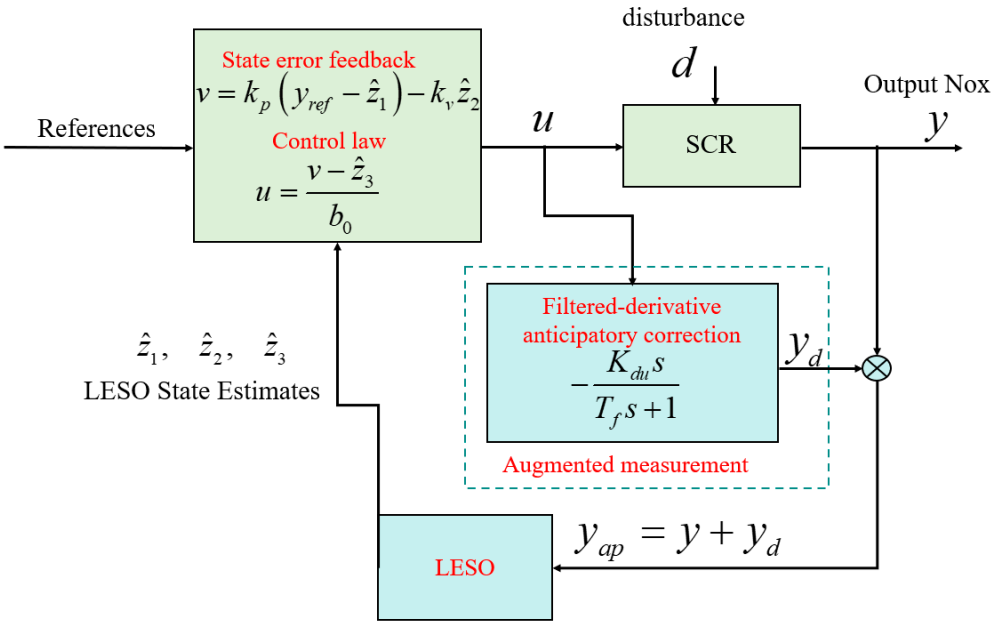


Figure 2. Control structure of the proposed AA-LADRC for SCR denitrification.

The filtered-derivative anticipatory process increment is defined in the frequency domain as

$$Y_d(s) = -K_{du}\frac{s}{T_f s + 1}U(s) \tag{15}$$

where $K_{du} > 0$ is the anticipatory gain, and $T_f > 0$ is the filter time constant. The negative sign is introduced according to the negative steady-state gain of the ammonia-injection control channel. The augmented measurement supplied to the LESO is defined as

$$Y_{ap}(s) = Y(s) + Y_d(s) = Y(s) - K_{du}\frac{s}{T_f s + 1}U(s) \tag{16}$$

To avoid direct numerical differentiation of the ammonia-injection command, an auxiliary low-pass-filter state is introduced, x_u, as

$$T_f\dot{x}_u + x_u = u \tag{17}$$

The augmented measurement incorporating the anticipatory process increment can be expressed in the time domain as

$$\begin{aligned} y_d &= -\tfrac{K_{du}}{T_f}(u - x_u) \\ y_{ap} &= y - \tfrac{K_{du}}{T_f}(u - x_u) \end{aligned} \tag{18}$$

Here, x_u represents the low-pass-filtered trend of the ammonia-injection command, whereas $u - x_u$ represents the transient deviation of the current input from its low-frequency trend. When the ammonia-injection command varies, this deviation generates a finite-bandwidth anticipatory process increment.

Using y_{ap} instead of the actual measurement y, the third-order LESO is given by

$$\begin{aligned} \dot{z}_1 &= z_2 + \beta_1(y_{ap} - z_1), \\ \dot{z}_2 &= z_3 + b_{i0}u + \beta_2(y_{ap} - z_1), \\ \dot{z}_3 &= \beta_3(y_{ap} - z_1). \end{aligned} \tag{19}$$

The actual SCR process and the known-input channel of the LESO are both driven by the actual ammonia-injection command, u. The proposed method only modifies the measurement channel of the observer by replacing the actual measurement, y, with the augmented measurement, y_{ap}.

The augmented measurement is

$$y_{ap} = y + y_d \tag{20}$$

The second derivative of the augmented measurement satisfies

$$\ddot{y}_{ap} = \ddot{y} + \ddot{y}_d = f_{ip} + b_{i0}u \tag{21}$$

where

$$f_{ip} = f_i + \ddot{y}_d \tag{22}$$

denotes the equivalent disturbance associated with the augmented-measurement dynamics. Therefore, under ideal continuous-time observation, the extended state satisfies

$$z_3 \approx f_{ip} = f_i + \ddot{y}_d \tag{23}$$

The term y_d is not explicitly calculated in the controller. Instead, its effect is implicitly reconstructed by the LESO through the augmented-measurement error.

The LADRC control law remains unchanged and is expressed as

$$u = \frac{v - z_3}{b_{i0}} \tag{24}$$

where the nominal virtual control is

$$v = k_p(y_{ref} - z_1) - k_v z_2 \tag{25}$$

When the LESO estimation errors are sufficiently small, one has

$$z_1 \approx y_{ap}, \quad z_2 \approx \dot{y}_{ap}, \quad z_3 \approx f_i + \ddot{y}_d \tag{26}$$

Substituting these relations into the actual SCR model gives

$$\ddot{y} = f_i + b_{i0}u \approx k_p(y_{ref} - y) - k_v\dot{y} - (k_p y_d + k_v\dot{y}_d + \ddot{y}_d) \tag{27}$$

Within the principal dynamic frequency range of the SCR process, the filtered-derivative operator can be interpreted from its low-frequency behavior. When $\omega T_f \ll 1$,

$$-K_{du}\frac{j\omega}{1 + j\omega T_f} \approx -K_{du}j\omega \tag{28}$$

Accordingly, the anticipatory process increment and augmented measurement approximately satisfy

$$y_d(t) \approx -K_{du}\dot{u}(t), \quad y_{ap}(t) \approx y(t) - K_{du}\dot{u}(t) \tag{29}$$

An important property of the filtered-derivative operator is its zero steady-state gain. Since

$$-K_{du}\frac{s}{T_f s + 1}\bigg|_{(s\,=\,0)} = 0 \tag{30}$$

the anticipatory process increment vanishes when the ammonia-injection command approaches a constant value. Consequently, the augmented measurement converges to the actual outlet measurement, indicating that the proposed anticipation augment mechanism reshapes only the transient information supplied to the LESO without altering the steady-state measurement.

The transient behavior can be further illustrated by considering a step variation in the ammonia-injection command. Suppose that the input changes by Δu at $t = t_0$. The corresponding anticipatory process increment is

$$y_d(t) = -\frac{K_{du}}{T_f}\Delta u \exp\left(-\frac{t-t_0}{T_f}\right), \quad t \geq t_0 \tag{31}$$

Its initial amplitude is therefore

$$y_d(t_0^+) = -\frac{K_{du}}{T_f}\Delta u \tag{32}$$

Thus, an input step immediately generates a transient measurement whose direction is consistent with the subsequent outlet NOx response. The ratio $\frac{K_{du}}{T_f}$ determines the initial anticipatory process increment amplitude, whereas T_f determines the decay timescale.

The frequency-domain characteristics further clarify the role of the filtered-derivative structure. Its magnitude is

$$\left|K_{du}\frac{j\omega}{1+j\omega T_f}\right| = \frac{K_{du}\omega}{\sqrt{1+\omega^2 T_f^2}} \tag{33}$$

and its high-frequency gain is bounded by

$$\lim_{\omega\to\infty}\left|K_{du}\frac{j\omega}{1+j\omega T_f}\right| = \frac{K_{du}}{T_f} \tag{34}$$

Unlike an ideal differentiator, whose magnitude increases without bound with frequency, the proposed filtered-derivative operator has a finite high-frequency gain. Hence, the variation trend of the ammonia-injection command can be extracted without introducing the unbounded high-frequency amplification inherent to direct differentiation.

The two parameters K_{du} and T_f play different but coupled roles. For frequencies satisfying $\omega \ll \frac{1}{T_f}$,

$$\left|K_{du}\frac{j\omega}{1+j\omega T_f}\right| \approx K_{du}\omega \tag{35}$$

indicating that K_{du} mainly determines the anticipatory process increment gain within the principal SCR dynamic range. In contrast, $1/T_f$ determines the transition frequency from derivative-like behavior to bounded-gain behavior, while $\frac{K_{du}}{T_f}$ determines both the initial anticipatory process increment amplitude under a step input and the upper bound of the high-frequency gain.

Increasing K_{du} strengthens the anticipatory process increment but simultaneously increases sensitivity to rapid input variations. Decreasing T_f accelerates the measurement dynamics and extends the derivative-like behavior toward higher frequencies, but it also increases the limiting gain $\frac{K_{du}}{T_f}$. Therefore, K_{du} and T_f should be jointly selected to balance the anticipatory process increment effect, measurement duration, and sensitivity to high-frequency input variations.

4. Lyapunov-Based Stability and Ultimate Boundedness Analysis

Under finite LESO estimation errors and time-varying generalized disturbances, the closed-loop stability of AA-LADRC requires further analysis. Section 3.2 explains the equivalent disturbance represented by the third observer state under ideal observation conditions, whereas this section further considers the nonzero estimation errors associated with a finite-bandwidth LESO. For the SCR denitrification process, the generalized disturbance mainly includes the internal process dynamics, inlet NOx variations, flue-gas flow-rate and

temperature fluctuations, input-gain uncertainty, and unmodeled dynamics. The following analysis is conducted over each time interval during which the reference signal remains constant. A finite reference step only causes a finite change in the tracking error and does not affect the continuous-time stability within the subsequent constant-reference interval.

Assumption 1. *The reference signal is constant over the considered interval, and the generalized disturbance, f_i, is continuously differentiable with a bounded derivative, i.e.,*

$$\left|\dot{f}_i(t)\right| \le \bar{h}, \quad 0 \le \bar{h} < \infty \tag{36}$$

For convenience, define $h(t) = \dot{f}_{i(t)}$.

Assumption 2. *The nominal input gain, $b_{i0} \neq 0$, has the same sign as the identified ammonia-injection control channel. The input-gain mismatch is incorporated into f_i, while persistent actuator amplitude or rate saturation is excluded from the basic stability analysis.*

Assumption 3. *The controller and filtered-derivative parameters satisfy*

$$k_p > 0, \quad k_v > 0, \quad T_f > 0, \quad K_{du} > 0 \tag{37}$$

and the LESO gains are selected as

$$\beta_1 = 3\omega_o, \quad \beta_2 = 3\omega_o^2, \quad \beta_3 = \omega_o^3, \quad \omega_o > 0 \tag{38}$$

The filtered-derivative anticipatory process increment and the augmented measurement supplied to the LESO are defined as

$$Y_d(s) = -K_{du}\frac{s}{T_f s + 1}U(s), \quad y_{ap} = y + y_d \tag{39}$$

The negative sign is consistent with the negative gain of the SCR ammonia-injection control channel, such that an increase in ammonia injection produces an anticipatory process increment consistent with the subsequent decrease in the outlet NOx concentration.

Define the tracking errors and observer-state deviations as

$$\begin{aligned} e_1 &= y - y_{ref}, \quad e_2 = \dot{y} \\ e_{o1} &= z_1 - y, \quad e_{o2} = z_2 - \dot{y}, \quad e_{o3} = z_3 - f_i \end{aligned} \tag{40}$$

Here, $e_{o3} = z_3 - f_i$ denotes the deviation of the third observer state from the original generalized disturbance. Since the augmented-measurement dynamics correspond to the equivalent disturbance, $f_p = f_i + \ddot{y}_d$, e_{o3} contains both the finite-bandwidth estimation error relative to f_p and the anticipatory process increment contribution, $\ddot{y}_d$. The nominal virtual control and LADRC control law are

$$v = -k_p e_1 - k_v e_2 - k_p e_{o1} - k_v e_{o2}, \quad u = \frac{v - z_3}{b_{i0}} \tag{41}$$

Since $z_3 = f_i + e_{o3}$, substituting the control law into $y = f_i + b_{i0}u$ gives the tracking-error dynamics:

$$\begin{aligned} \dot{e}_1 &= e_2 \\ \dot{e}_2 &= -k_p e_1 - k_v e_2 - k_p e_{o1} - k_v e_{o2} - e_{o3} \end{aligned} \tag{42}$$

For the augmented-measurement LESO, the observer-error dynamics are

$$\begin{aligned} \dot{e}_{o1} &= -\beta_1 e_{o1} + e_{o2} + \beta_1 y_d \\ \dot{e}_{o2} &= -\beta_2 e_{o1} + e_{o3} + \beta_2 y_d \\ \dot{e}_{o3} &= -\beta_3 e_{o1} + \beta_3 y_d - h(t) \end{aligned} \tag{43}$$

Unlike the conventional LESO, the anticipatory process increment, y_d, directly affects the observer-error dynamics because the measurement update is based on $y_{ap} = y + y_d$.

The filtered-derivative relation is equivalently written in the time domain as

$$T_f \dot{y}_d + y_d = -K_{du} \dot{u} \tag{44}$$

Differentiating the control law first gives

$$\dot{u} = \frac{1}{b_{i0}} \left(-k_p \dot{e}_1 - k_v \dot{e}_2 - k_p \dot{e}_{o1} - k_v \dot{e}_{o2} - \dot{z}_3 \right) \tag{45}$$

Using $z_3 = e_{o3} + f_i$, $h(t) = \dot{f}_i$ and the tracking- and observer-error dynamics in (42) and (43), the above expression can be rearranged as

$$\dot{u} = l_c^T e_c + l_o^T e_o + l_y y_d \tag{46}$$

where

$$e_c = [e_1 \; e_2]^T, \quad e_o = [e_{o1} \; e_{o2} \; e_{o3}]^T \tag{47}$$

and

$$\begin{aligned} l_c &= \frac{1}{b_{i0}} \begin{bmatrix} k_p k_v \\ k_v^2 - k_p \end{bmatrix} \\ l_o &= \frac{1}{b_{i0}} \begin{bmatrix} k_p k_v + k_p \beta_1 + k_v \beta_2 + \beta_3 \\ k_v^2 - k_p \\ 0 \end{bmatrix} \\ l_y &= -\frac{k_p \beta_1 + k_v \beta_2 + \beta_3}{b_{i0}} \end{aligned} \tag{48}$$

For the SCR ammonia-injection control channel, $b_{i0} < 0$, and therefore $l_y > 0$.

Define

$$\kappa_{du} = \frac{K_{du}}{T_f}, \quad a_f = \frac{1}{T_f} + \kappa_{du} l_y \tag{49}$$

where κ_{du} denotes the effective anticipatory gain.

Since $T_f > 0$, $\kappa_{du} > 0$, and $l_y > 0$, one has $a_f > 0$.

For compactness, define

$$A_c = \begin{bmatrix} 0 & 1 \\ -k_p & -k_v \end{bmatrix}, \quad B_c = \begin{bmatrix} 0 & 0 & 0 \\ -k_p & -k_v & -1 \end{bmatrix} \tag{50}$$

and

$$A_o = \begin{bmatrix} -\beta_1 & 1 & 0 \\ -\beta_2 & 0 & 1 \\ -\beta_3 & 0 & 0 \end{bmatrix}, \quad g_y = \begin{bmatrix} \beta_1 \\ \beta_2 \\ \beta_3 \end{bmatrix}, \quad E_o = \begin{bmatrix} 0 \\ 0 \\ -1 \end{bmatrix} \tag{51}$$

Define the complete augmented error vector as

$$X = \begin{bmatrix} e_c^T & e_o^T & y_d \end{bmatrix}^T \tag{52}$$

Combining the tracking-error, observer-error, and anticipatory process increment dynamics gives

$$\dot{X} = A_p X + E_p h(t) \tag{53}$$

where

$$A_p = \begin{bmatrix} A_c & B_c & 0_{2\times 1} \\ 0_{3\times 2} & A_o & g_y \\ -\kappa_{du} l_c^T & -\kappa_{du} l_o^T & -a_f \end{bmatrix}, \quad E_p = \begin{bmatrix} 0_{2\times 1} \\ E_o \\ 0 \end{bmatrix} \tag{54}$$

Since $a_f = \frac{1}{T_f} + \kappa_{du} l_y$, the augmented matrix depends affinely on κ_{du} and can be written as

$$A_p = A_0 + \kappa_{du} A_1, \quad A_0 = A_p\big|_{\kappa_{du}=0}, \quad A_1 = \frac{\partial A_p}{\partial \kappa_{du}} \tag{55}$$

In particular,

$$A_1 = \begin{bmatrix} 0_{2\times 2} & 0_{2\times 3} & 0_{2\times 1} \\ 0_{3\times 2} & 0_{3\times 3} & 0_{3\times 1} \\ -l_c^T & -l_o^T & -l_y \end{bmatrix} \tag{56}$$

When $\kappa_{du} = 0$, A_0 is block upper triangular, and its characteristic polynomial is

$$\det(sI - A_0) = (s^2 + k_v s + k_p)(s + \omega_o)^3 \left(s + \frac{1}{T_f}\right) \tag{57}$$

Therefore, A_0 is Hurwitz under Assumption 3. For $\kappa_{du} > 0$, the stability of the complete anticipation augment closed loop is determined directly from the augmented matrix, A_p.

Theorem 1. *Suppose that Assumptions 1–3 hold and that K_{du} and T_f are selected such that the complete augmented matrix, A_p, is Hurwitz. Then, the augmented error state, X, is uniformly ultimately bounded under the bounded disturbance-rate condition in Assumption 1. Moreover, if $\dot{f}_{i(t)} \equiv 0$, then X converges exponentially to the origin.*

Proof. Since A_p is Hurwitz, for any prescribed symmetric positive-definite matrix $Q_p = Q_p^T > 0$, there exists a unique symmetric positive-definite matrix $P_p = P_p^T > 0$ satisfying

$$A_p^T P_p + P_p A_p = -Q_p \tag{58}$$

Consider the Lyapunov function,

$$V = X^T P_p X \tag{59}$$

Its derivative along the trajectories of (53) is

$$\dot{V} = -X^T Q_p X + 2X^T P_p E_p h(t) \tag{60}$$

Define

$$\underline{p} = \lambda_{\min}(P_p), \quad \overline{p} = \lambda_{\max}(P_p), \quad q_p = \lambda_{\min}(Q_p), \quad \gamma_h = \left\| P_p E_p \right\|_2 \tag{61}$$

Using $|h(t)| \le \overline{h}$ and Young's inequality gives

$$\dot{V} \le -q_p \|X\|^2 + 2\gamma_h \overline{h} \|X\| \le -\frac{q_p}{2}\|X\|^2 + \frac{2\gamma_h^2}{q_p}\overline{h}^2 \le -\lambda V + c_h \overline{h}^2 \tag{62}$$

where

$$\lambda = \frac{q_p}{2\overline{p}}, \quad c_h = \frac{2\gamma_h^2}{q_p} \tag{63}$$

According to the comparison principle,

$$V(t) \le e^{-\lambda t} V(0) + \frac{c_h \overline{h}^2}{\lambda}\left(1 - e^{-\lambda t}\right) \tag{64}$$

Since

$$\underline{p}\|X\|^2 \le V \le \overline{p}\|X\|^2 \tag{65}$$

it follows that

$$\limsup_{t\to\infty} \|X(t)\| \le \overline{h}\sqrt{\frac{c_h}{\lambda \underline{p}}} \tag{66}$$

Hence, the tracking errors, LESO estimation errors, and anticipatory process increment state are uniformly ultimately bounded.

When $\dot{f}_{i(t)} \equiv 0$, one has $h(t) \equiv 0$, and

$$\dot{V} \leq -\frac{q_p}{\bar{p}} V \tag{67}$$

Therefore,

$$V(t) \leq \exp\left(-\frac{q_p}{\bar{p}} t\right) V(0), \quad X(t) \to 0 \tag{68}$$

which establishes exponential stability under a constant reference and a constant generalized disturbance. □

Theorem 1 shows that the proposed AA-LADRC preserves uniform ultimate boundedness of the augmented error vector, X, under bounded generalized-disturbance variation, provided that the complete augmented matrix is Hurwitz. This result applies to the tracking errors, observer-state deviations, and anticipatory process increment state included in X, rather than to every internal signal of the closed-loop system.

5. Simulation Results and Discussion

The industrial SCR model identified in [17] from a 300 MW coal-fired unit is used for simulation. Four disturbance scenarios are considered: inlet NOx step, composite inlet NOx, outlet NOx, and ammonia-injection disturbances. PI, LADRC, and AA-LADRC are compared under identical plant parameters, initial conditions, and actuator constraints, with the widely used PI controller adopted as the industrial baseline and LADRC serving as the direct ADRC comparator. The control configuration used for these disturbance-rejection tests is shown in Figure 3.

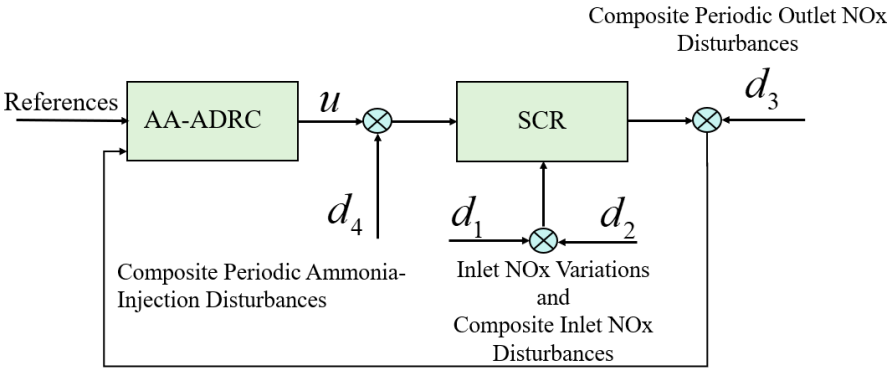


Figure 3. Control configuration of the SCR system for inlet NOx variation and multiple disturbance-rejection tests.

5.1. Controller Parameter Tuning

To evaluate the closed-loop tracking and disturbance-rejection performance of the proposed method, the industrially identified SCR model listed in Table 1 is adopted as the simulation plant. For the identified second-order ammonia-injection control channel, the nominal control gain is determined from the identified model parameters as

$$b_{i0} = \frac{K_u}{T_1 T_2} \tag{69}$$

where the sign of b_{i0} is selected to be consistent with the identified ammonia-injection control channel.

Table 1. Industrially identified transfer-function models of the SCR system.

Channel	Identified Transfer Function
$G_u(s)$	$\frac{-0.650}{(303.66s+1)(84.10s+1)}$
$G_d(s)$	$\frac{0.383}{251.42s+1}$

The feedback gains are tuned using the bandwidth-parameterization method. By assigning the desired closed-loop characteristic polynomial as $(s+\omega_c)^2$, the feedback gains are obtained as

$$k_p = \omega_c^2, \quad k_v = 2\omega_c \tag{70}$$

where ω_c denotes the controller bandwidth.

Because the identified ammonia-injection control channel has a relative degree of two, a third-order LESO is employed. By assigning the observer characteristic polynomial as $(s+\omega_o)^3$, the observer gains are determined as

$$\beta_1 = 3\omega_o, \quad \beta_2 = 3\omega_o^2, \quad \beta_3 = \omega_o^3 \tag{71}$$

where ω_o denotes the observer bandwidth.

The filter time constant $T_f > 0$ is first selected according to the dominant dynamic timescale of the identified SCR process.

For the AA-LADRC structure, the complete augmented matrix is written as

$$A_p = A_0 + \kappa_{du} A_1, \quad \kappa_{du} = \frac{K_{du}}{T_f} \tag{72}$$

where A_0 and A_1 are the baseline augmented matrix and the anticipatory process increment gain dependent matrix defined in Section 4, respectively.

For a given T_f, κ_{du} is selected by evaluating the eigenvalues of the corresponding A_p. According to Theorem 1, the selected parameters are admissible if A_p is Hurwitz, i.e.,

$$\max_i \mathrm{Re}\left[\lambda_i(A_p)\right] < 0 \tag{73}$$

Once an admissible κ_{du} has been obtained, K_{du} is determined as

$$K_{du} = T_f \kappa_{du} \tag{74}$$

For all simulations, the rated-load condition $N = N_E$ is assumed, with the nominal operating point $u_0 = 122.923$ kg/h, $d_0 = 300$ mg/Nm^3, and $y_{ref} = 35$ mg/Nm^3. The plant dynamics are initialized at the steady state corresponding to the nominal operating point. The PI gains were tuned under the nominal operating condition to achieve a relatively fast dynamic response while maintaining a small steady-state error, yielding $K_p = 13.33$ and $K_i = 0.01882$, and the integral state was initialized at u_0. LADRC and AA-LADRC use $\omega_c = 0.009$ rad/s and $\omega_o = 0.018$ rad/s, while AA-LADRC additionally uses $K_{du} = 10$ and $T_f = 80$ s. All controllers are implemented with $T_s = 10$ s, $122 \le u \le 160$ kg/h, and $|\Delta u| \le 10$ kg/h per sampling interval. The LESO is initialized as $z_1(0) = y_{ref}$, $z_2(0) = 0$, and $z_3(0) = -b_{i0}u_0$. For this parameter set, $\max \mathrm{Re}\{\lambda(A_p)\} = -8.62\times10^{-4} < 0$, confirming that the complete augmented matrix is Hurwitz. The LESO is discretized using the forward-Euler method; the PI controller employs conditional-integration/back-calculation anti-windup; and the discrete anticipatory process increment is constructed from the two previous constrained ammonia commands, with the filtered input-rate state, δ_u, initialized to zero and both stored ammonia commands initialized to u_0, corresponding to $x_u(0) = u_0$ and a zero initial anticipatory increment, $y_d(0) = 0$.

The computation and update sequence of the controllers and the SCR plant within each sampling interval is summarized in Algorithm 1.

Algorithm 1. Sampled update of the SCR plant and controllers.

Initialize: Set the plant states to the nominal steady state;

$T_s = 10\,\text{s}$, $\alpha = \frac{T_f}{T_f+T_s}$, $z = (y_{\text{ref}}, 0, -b_{i0}u_0)^{\text{T}}$, $I = u_0$, $\delta_u = 0$, $h_1 = h_2 = u_0$.

For each sampling instant $k = 0, 1, \ldots$:

Acquire the outlet-NOx feedback measurement y_m.

If PI is used:

Compute the candidate integral contribution and control command:

$$e = y_m - y_{\text{ref}}, \quad I^* = I + K_i T_s e, \quad u^* = K_p e + I^*.$$

Else:

If LADRC is used: Set $y_d = 0$**.**

If AA-LADRC is used:

$$\delta_u \leftarrow \alpha\delta_u + (1-\alpha)\frac{h_1 - h_2}{T_s}, \quad y_d = -K_{du}\delta_u.$$

Set $\varepsilon = z_1 - (y_m + y_d)$ and simultaneously update:

$$z \leftarrow z + T_s \begin{bmatrix} z_2 - \beta_1\varepsilon \\ z_3 + b_{i0}h_1 - \beta_2\varepsilon \\ -\beta_3\varepsilon \end{bmatrix}.$$

Compute the command using the updated states:

$$u^* = \frac{k_p(y_{\text{ref}} - z_1) - k_v z_2 - z_3}{b_{i0}}.$$

End if.

Apply the command-increment and magnitude limits sequentially:

$$u^r = h_1 + \min\left(\max(u^* - h_1, -10), 10\right), \quad u = \min\left(\max(u^r, 122), 160\right).$$

If PI is used:

If neither limit is active: $I \leftarrow I^*$**;**

Else if $u = 160$: Set $I \leftarrow I^*$ **only if** $e < 0$; otherwise retain I;

ELse if $u = 122$**: Set** $I \leftarrow I^*$ **only if** $e > 0$**; otherwise retain** I**;**

Else: $I \leftarrow u - K_p e$.

End if.

Advance the plant states and sequentially update the command history:

$$h_2 \leftarrow h_1, \quad h_1 \leftarrow u.$$

End for.

In Algorithm 1, h_1 and h_2 store the previous and second-previous constrained ammonia commands, respectively; δ_u is the filtered input-rate state; I and I^* denote the stored and candidate integral contributions; and u^* and u^r denote the unconstrained and increment-limited commands. The symbol "$\leftarrow$" denotes assignment. The anticipatory path uses the two previous constrained commands and thus introduces a one-sample delay relative to the current input increment. The LESO uses the previous constrained command, while the control law uses the observer states updated within the current sampling interval. All controllers apply the command-increment limit before the magnitude limit. For PI, integration proceeds normally when neither limit is active. At a magnitude bound, integration is permitted only when it helps the command leave saturation; otherwise, the previous integral contribution is retained. When only increment limiting is active and the command remains strictly within the magnitude bounds, the integral contribution is recalculated from the constrained command:

$$I_k = \begin{cases} I_k^*, & u_k^* = u_k^r = u_k, \\ I_k^*, & u_k = 160,\ e_k < 0, \\ I_k^*, & u_k = 122,\ e_k > 0, \\ u_k - K_p e_k, & 122 < u_k < 160, \\ I_{k-1}, & \text{otherwise.} \end{cases} \tag{75}$$

The branches are evaluated in the order shown, with the first satisfied condition applied. Here, $I_k^* = I_{k-1} + K_i T_s e_k$, and the subscript k, omitted from Algorithm 1 for brevity, denotes the sampling instant.

5.2. Disturbance Rejection Under Inlet NOx Variations

To evaluate the disturbance-rejection capability of the proposed method under a sudden variation in the inlet NOx concentration, the outlet NOx setpoint was maintained at 35 mg/Nm^3, while the inlet NOx concentration was increased stepwise, from 300 mg/Nm^3 to 330 mg/Nm^3. The initial ammonia-injection flow rate was set to 122.923 kg/h. The sampling period for the controllers, LESO, and SCR simulation was $T_s = 10$ s.

To quantitatively evaluate the disturbance-rejection performance, the outlet NOx tracking error is defined as

$$e(t) = y(t) - y_{ref} \tag{76}$$

where $e(t)$ denotes the outlet NOx tracking error, $y(t)$ denotes the outlet NOx signal used for performance evaluation, $y_{true}(t)$ is the true SCR outlet NOx concentration before the externally imposed measurement disturbance, and $y_{ref} = 35$ mg/Nm^3 is the reference value. When the measurement disturbance $d_3\ (t)$ is present, $y(t) = y_{true}(t) + d_3(t)$; otherwise, $y(t) = y_{true}(t)$. The same measurement disturbance is applied to all three controllers to ensure a consistent comparison.

The maximum absolute deviation, e_{max}; Root-Mean-Square Error (RMSE); post-peak recovery time, t_r; and total variation in the ammonia-injection command, TV_u, are selected as the performance indices. The maximum absolute deviation is defined as

$$e_{\max} = \max_{t\in[0,T]} \left|e(t)\right| \tag{77}$$

where T denotes the end time of the evaluation interval.

The RMSE is defined as

$$RMSE = \sqrt{\frac{1}{T}\int_0^T e^2(t)dt} \tag{78}$$

The TV_u is defined as

$$TV_u = \int_0^T \left|\dot{u}(t)\right| dt \tag{79}$$

where $u(t)$ denotes the controller-generated ammonia-injection command before the externally imposed actuator disturbance. Here, e_{max} characterizes the peak disturbance deviation, RMSE reflects the overall tracking-error level, t_r characterizes the post-peak recovery speed, and TV_u quantifies the cumulative variation in the ammonia-injection command over the evaluation interval. A smaller TV_u indicates a smoother control action with less overall command variation. The total variation is calculated from consecutive constrained ammonia-command samples, including all discrete command jumps within the evaluation interval. The performance indices in Sections 5.2–5.5 are evaluated over 0–2000 s, while those in Section 5.6 are evaluated over 0–5000 s.

The time instant at which the response enters and subsequently remains within the prescribed error band after the occurrence of the maximum absolute deviation is defined as

$$t_s = \min\left\{t \geq t_p : \left|e(\tau)\right| \leq \Delta e,\ \forall \tau \in [t, T]\right\} \tag{80}$$

and the post-peak recovery time is defined as

$$t_r = t_s - t_p \tag{81}$$

where t_p is the time instant at which e_{max} occurs, t_s is the time instant at which the response enters and remains within the prescribed error band, τ is the time variable, and $\Delta e = 0.7$ mg/Nm^3 is the allowable error bound. The recovery band is set to 0.7 mg/Nm^3 and is used only as a common threshold for comparing post-peak recovery speed. Therefore, t_r characterizes the dynamic recovery speed after the peak deviation.

To compare the transient responses of the third LESO state, Z_3, its deviation from the steady-state value is normalized as follows:

$$\overline{Z}_3(t) = \frac{Z_3(t) - Z_3^{ss}}{\max|Z_3(t) - Z_3^{ss}|} \tag{82}$$

where Z_3^{ss} denotes the corresponding steady-state value. A common normalization factor is used for both LESOs to preserve their relative deviation amplitudes and facilitate comparison of their transient settling behavior.

Figure 4 and Table 2 present the dynamic responses and quantitative performance comparison of PI, LADRC, and AA-LADRC under the inlet NOx step disturbance. The three controllers exhibit comparable maximum absolute deviations, with AA-LADRC yielding the smallest value of 2.69 mg/Nm^3. Its RMSE is 0.73 mg/Nm^3, slightly lower than 0.76 mg/Nm^3 for PI and markedly lower than 1.11 mg/Nm^3 for LADRC. More importantly, AA-LADRC shortens the recovery time to 170 s, compared with 440 s for PI and 730 s for LADRC, showing that its main advantage lies in faster post-peak error attenuation and dynamic recovery. Conventional LADRC mainly relies on the current output-measurement error for observer measurement, whereas AA-LADRC incorporates the transient variation information of the ammonia-injection command into the LESO measurement channel. Figure 5 shows the normalized response of the third LESO state, Z_3. As reported in Table 3, the 5% settling time of AA-LADRC decreases from 120 s for conventional LADRC to 40 s, representing a reduction of 66.7% and indicating faster settling during the investigated initial transient.

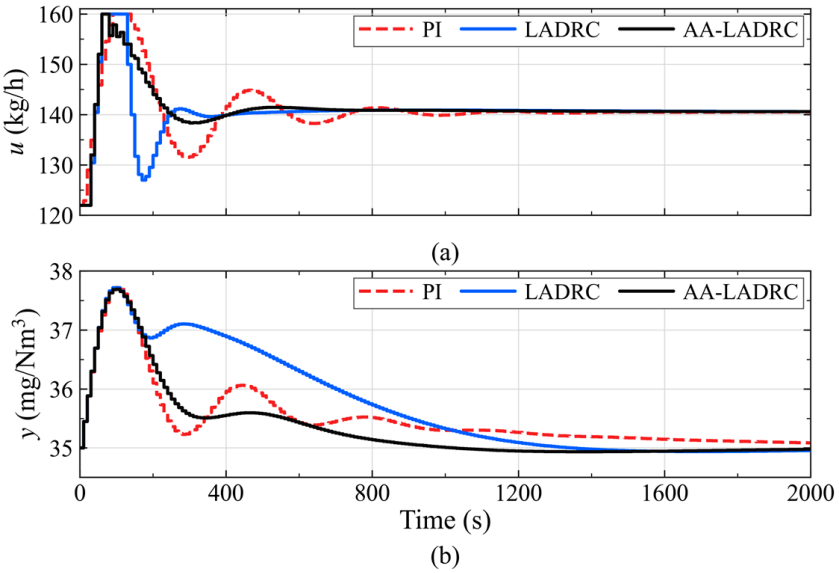


Figure 4. Disturbance-rejection responses of PI, LADRC, and AA-LADRC when the inlet NOx concentration increases stepwise, from 300 mg/Nm^3 to 330 mg/Nm^3: (**a**) ammonia-injection control signal and (**b**) outlet NOx concentration.

Table 2. Performance comparison of PI, LADRC, and AA-LADRC when the inlet NOx concentration increases stepwise, from 300 mg/Nm^3 to 330 mg/Nm^3.

Performance Index	PI	LADRC	AA-LADRC
e_{max} (mg/Nm^3)	2.72	2.72	2.69
RMSE (mg/Nm^3)	0.76	1.11	0.73
t_r (s)	440	730	170
TV_u (kg/h)	92.44	88.30	69.61

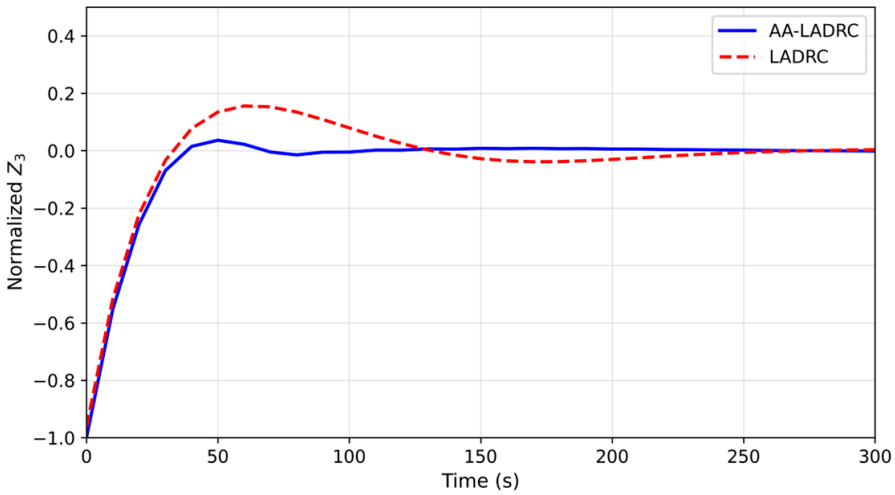


Figure 5. Comparison of the normalized third observer-state, Z_3, responses of LADRC and AA-LADRC during the initial transient.

Table 3. Comparison of the transient settling performance of the third LESO state.

Performance Index	LADRC	AA-LADRC
5% settling time (s)	120	40

The total variation in the ammonia-injection command is 69.61 kg/h for AA-LADRC, lower than 92.44 kg/h for PI and 88.30 kg/h for LADRC. The faster recovery is accompanied by a smaller cumulative variation in the ammonia-injection command. The finite-bandwidth anticipatory process increment acts mainly during changes in the control input, allowing input-variation information to participate in the LESO measurement and yielding smoother ammonia-injection regulation while preserving the observed transient response.

5.3. Disturbance-Rejection Performance Under Composite Inlet NOx Disturbances

A composite step–periodic disturbance was introduced into the inlet NOx concentration. The inlet NOx concentration was increased stepwise from 300 mg/Nm^3 to 330 mg/Nm^3, while a multi-frequency periodic disturbance was simultaneously superimposed on the inlet signal. The outlet NOx setpoint was maintained at 35 mg/Nm^3. The initial ammonia-injection flow rate was set to 122.923 kg/h, and the sampling period was 10 s.

The composite inlet disturbance is defined as

$$c_1(t) = c_{1,\text{step}}(t) + d_{\text{per}}(t) \tag{83}$$

where $c_{1,step}(t)$ represents the inlet NOx step variation, and $d_{per}(t)$ denotes the periodic disturbance component. The periodic disturbance component is constructed as

$$d_{\text{per}}(t) = \sum_{i=1}^{3} A_i \sin(\omega_i t + \phi_i) \tag{84}$$

where A_i, ω_i, and φ_i represent the amplitude, angular frequency, and initial phase of each sinusoidal component, respectively. The corresponding angular frequencies are defined as

$$\omega_i = \frac{2\pi}{P_i}, \quad i = 1, 2, 3 \tag{85}$$

In this test, the disturbance parameters were selected as $A_1 = 1.5$ mg/Nm^3, $A_2 = 0.8$ mg/Nm^3, and $A_3 = 0.4$ mg/Nm^3, with periods of $P_1 = 1000$ s, $P_2 = 500$ s, and $P_3 = 250$ s. The initial phases were set as $\varphi_1 = 0$, $\varphi_2 = \frac{\pi}{3}$, and $\varphi_3 = \frac{\pi}{5}$.

Figure 6 and Table 4 present the dynamic responses and quantitative performance comparison of PI, LADRC, and AA-LADRC under the composite inlet NOx disturbance. AA-LADRC reduces the maximum absolute deviation to 3.08 mg/Nm^3, compared with 3.09 mg/Nm^3 for PI and 3.23 mg/Nm^3 for LADRC. Its RMSE is 1.33 mg/Nm^3, lower than the 1.56 mg/Nm^3 obtained by LADRC but higher than the 0.97 mg/Nm^3 obtained by PI. During the sustained multi-frequency periodic disturbance, AA-LADRC maintains a smaller peak deviation and suppresses the periodic fluctuation of the outlet NOx concentration more effectively than LADRC.

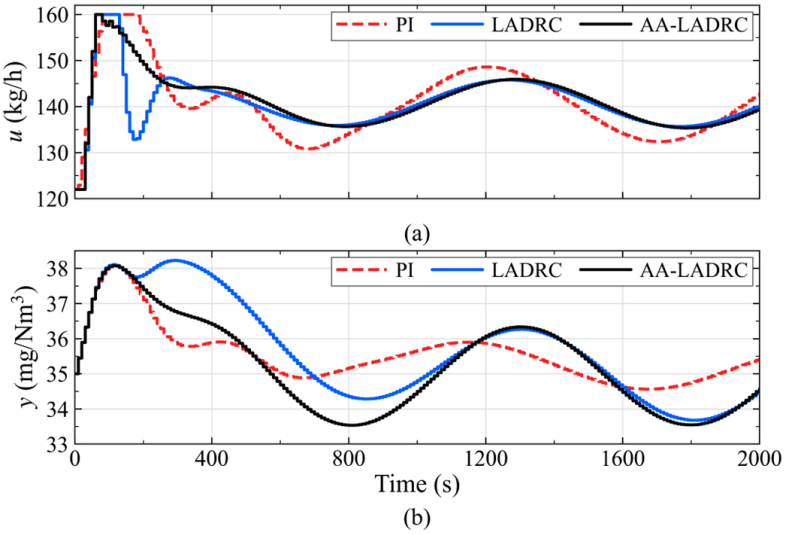


Figure 6. Disturbance-rejection responses of PI, LADRC, and AA-LADRC under the composite step–periodic inlet NOx disturbance: (**a**) ammonia-injection control signal and (**b**) outlet NOx concentration.

Table 4. Performance comparison of PI, LADRC, and AA-LADRC under the composite step–periodic inlet NOx disturbance.

Performance Index	PI	LADRC	AA-LADRC
e_{max} (mg/Nm^3)	3.09	3.23	3.08
RMSE (mg/Nm^3)	0.97	1.56	1.33
TV_u (kg/h)	118.44	113.33	89.77

The lower RMSE of PI is mainly associated with its direct and continuous measurement based on the instantaneous tracking error, which results in more frequent adjustments of the ammonia-injection command under sustained periodic disturbances. AA-LADRC places greater emphasis on utilizing transient input-side information while maintaining control smoothness. Its total variation in the ammonia-injection command decreases to 89.77 kg/h, compared with 118.44 kg/h for PI and 113.33 kg/h for LADRC. AA-LADRC therefore achieves a comparable maximum deviation to PI with substantially smaller control variation, providing smoother ammonia-injection regulation for the large-inertia and dynamic-lag characteristics of the SCR process.

5.4. Disturbance-Rejection Performance Under Composite Periodic Outlet NOx Disturbances

A composite periodic disturbance was superimposed on the outlet NOx signal to evaluate the closed-loop disturbance-rejection performance under measurement fluctuations. The disturbance adopted the same three-frequency sinusoidal composition and parameters as those used in Section 5.3, and all other simulation settings were kept unchanged.

Figure 7 and Table 5 present the dynamic responses and quantitative performance comparison of PI, LADRC, and AA-LADRC under the composite periodic outlet NOx measurement disturbance. AA-LADRC yields a maximum absolute deviation of 3.90 mg/Nm^3, close to 3.91 mg/Nm^3 for LADRC but higher than 3.70 mg/Nm^3 for PI. Its RMSE is 1.33 mg/Nm^3, lower than 1.57 mg/Nm^3 for LADRC but slightly higher than 1.25 mg/Nm^3 for PI. In this condition, the disturbance is directly superimposed on the outlet measurement channel and continuously enters the feedback loop, which tends to induce repeated adjustments of the ammonia-injection command. PI can reduce the output error through more direct and frequent adjustment of the control input, leading to a lower RMSE. AA-LADRC uses the variation in the controller-generated input to construct the anticipatory process increment, allowing input-side dynamic information to participate earlier in the LESO measurement. The externally imposed outlet-NOx measurement disturbance, d_3, is superimposed on the measured output supplied to the LESO and therefore enters through the measurement channel rather than the plant-side generalized-disturbance channel.

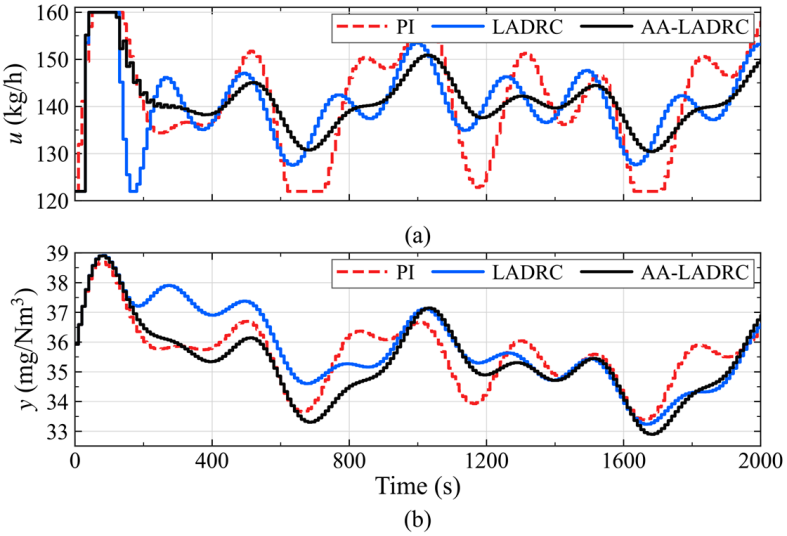


Figure 7. Disturbance-rejection responses of PI, LADRC, and AA-LADRC under the composite periodic outlet NOx measurement disturbance: (**a**) ammonia-injection control signal and (**b**) outlet NOx concentration.

Table 5. Performance comparison of PI, LADRC, and AA-LADRC under the composite periodic outlet NOx measurement disturbance.

Performance Index	PI	LADRC	AA-LADRC
e_{max} (mg/Nm^3)	3.70	3.91	3.90
RMSE (mg/Nm^3)	1.25	1.57	1.33
TV_u (kg/h)	312.27	285.42	170.56

The total variation in the ammonia-injection command is reduced to 170.56 kg/h for AA-LADRC, compared with 312.27 kg/h for PI and 285.42 kg/h for LADRC. The reduction is particularly significant under measurement disturbances because corrupted feedback can easily trigger unnecessary control adjustments. AA-LADRC suppresses these repeated

variations in the ammonia-injection command while maintaining an RMSE close to that of PI and clearly lower than that of LADRC. This indicates that its main advantage under persistent multi-frequency measurement disturbances lies in weakening the transmission of measurement fluctuations to the actuator and achieving substantially smoother ammonia-injection regulation.

5.5. Disturbance-Rejection Performance Under Composite Periodic Ammonia-Injection Disturbances

A composite periodic disturbance, d_4, was superimposed on the ammonia-injection control channel to evaluate the closed-loop disturbance-rejection performance under actuator-side disturbances. The actual ammonia flow applied to the SCR plant is therefore given by $u_p = u + d_4$, where u is the ammonia-injection command generated by the controller. The same disturbance, d_4, is applied to PI, LADRC, and AA-LADRC. Since d_4 is identical for all three controllers, the total variation in the controller-generated command, u, rather than the actual ammonia flow, u_p, is used to evaluate and compare their control effort and smoothness. The disturbance adopted the same three-frequency sinusoidal composition, periods, and initial phases as the periodic disturbance component used in Section 5.3. The LESO known-input channel and the anticipatory process increment channel use u, while the effect of d_4 is included in the generalized disturbance. All other simulation settings were kept unchanged.

Figure 8 and Table 6 present the dynamic responses and quantitative performance comparison of PI, LADRC, and AA-LADRC under the composite periodic ammonia-injection disturbance. AA-LADRC achieves an RMSE of 0.62 mg/Nm^3, lower than 0.73 mg/Nm^3 for PI and 0.93 mg/Nm^3 for LADRC. Its maximum absolute deviation is 2.43 mg/Nm^3, which is nearly identical to the 2.41 mg/Nm^3 obtained by LADRC and lower than the 2.62 mg/Nm^3 obtained by PI. Under this condition, the disturbance acts directly on the ammonia-injection control channel and varies periodically, requiring continuous adjustment of the ammonia-injection command to counteract its effect on the outlet NOx concentration. The anticipatory process increment channel is constructed from variations in the controller-generated ammonia-injection command, whereas the externally imposed actuator disturbance is handled through the plant-side generalized-disturbance channel. Under this configuration, AA-LADRC achieves a lower overall output error while maintaining a comparable peak deviation under the investigated periodic actuator-disturbance condition.

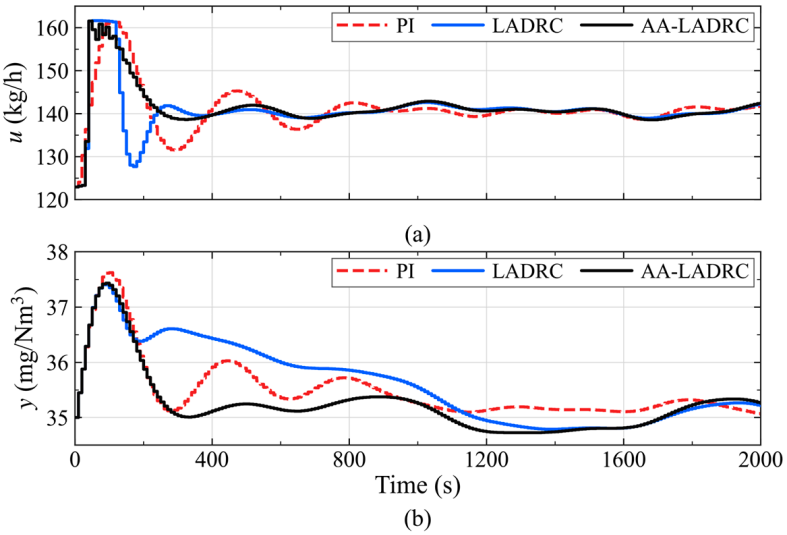


Figure 8. Disturbance-rejection responses of PI, LADRC, and AA-LADRC under the composite periodic ammonia-injection disturbance: (**a**) ammonia-injection flow rate and (**b**) outlet NOx concentration.

Table 6. Performance comparison of PI, LADRC, and AA-LADRC under the composite periodic ammonia-injection disturbance.

Performance Index	PI	LADRC	AA-LADRC
e_{max} (mg/Nm^3)	2.62	2.41	2.43
RMSE (mg/Nm^3)	0.73	0.93	0.62
TV_u (kg/h)	112.08	105.27	94.20

The total variation in the ammonia-injection command is 94.20 kg/h for AA-LADRC, lower than 112.08 kg/h for PI and 105.27 kg/h for LADRC. For a persistent periodic disturbance acting on the actuator channel, the smaller total variation indicates that the improved output performance is not obtained through frequent or large-amplitude adjustments of the ammonia-injection command. AA-LADRC achieves the lowest RMSE among the three controllers while maintaining the smallest cumulative variation in the control input, indicating improved disturbance-rejection performance together with smoother control action under this actuator-disturbance condition.

5.6. Sensitivity Test Under Synchronous ±10% Variations in the Two Plant Time Constants

To illustrate the sensitivity of the controllers to a slow change in the response speed of the ammonia-injection channel, the two dominant time constants are varied synchronously as $T_1(t) = T_{1,0}[1 + \delta_T \sin(2\pi t/T_v)]$ and $T_2(t) = T_{2,0}[1 + \delta_T \sin(2\pi t/T_v)]$, where $\delta_T = 0.10$, and $T_v = 2000$ s is the variation period. This period is approximately 6.6 and 23.8 times the two nominal time constants, respectively, and is selected to introduce relatively slow parameter variations. In practical operation, load adjustments cause changes in flue-gas flow rate and temperature, affecting gas residence time, catalytic reactions, and ammonia-storage dynamics, thereby altering the response speed of the SCR ammonia-injection channel. To represent such local dynamic changes around the nominal operating condition, synchronous ±10% variations in the two time constants are selected. Controller performance is evaluated under this specific variation scenario. The inlet NOx concentration is initially maintained at 300 mg/Nm^3, and is then repeatedly stepped between 330 mg/Nm^3 and 270 mg/Nm^3, with each level maintained for 500 s. The simulation horizon is extended to 5000 s to cover multiple cycles of the time-varying plant dynamics.

Figure 9 and Table 7 present the dynamic responses and quantitative performance comparison of PI, LADRC, and AA-LADRC under synchronous ±10% variations in the two plant time constants. As shown in the results, all three controllers maintain stable closed-loop responses throughout the test, indicating that the considered parameter variation does not lead to evident closed-loop instability. Compared with PI and conventional LADRC, AA-LADRC does not exhibit a uniform advantage in the output-error indices, with its maximum absolute deviation and RMSE remaining at comparable or slightly higher levels. Under the considered synchronous time-constant variation and repeated inlet-NOx step disturbances, the effect of the anticipation augment mechanism is therefore reflected less in further reducing the output error and more in modifying the variation characteristics of the control action.

In terms of ammonia-injection smoothness, AA-LADRC retains a clear advantage, with a substantially lower total variation in the control command than that of PI and conventional LADRC. Compared with LADRC, AA-LADRC reduces TV_u by approximately 29.68%. Thus, in this sensitivity case, the anticipatory process increment mechanism suppresses frequent and large-amplitude ammonia-injection adjustments, resulting in a smoother control input while maintaining stable closed-loop operation and acceptable regulation performance.

This behavior reflects the trade-off between disturbance-rejection accuracy and ammonia-injection smoothness in this case.

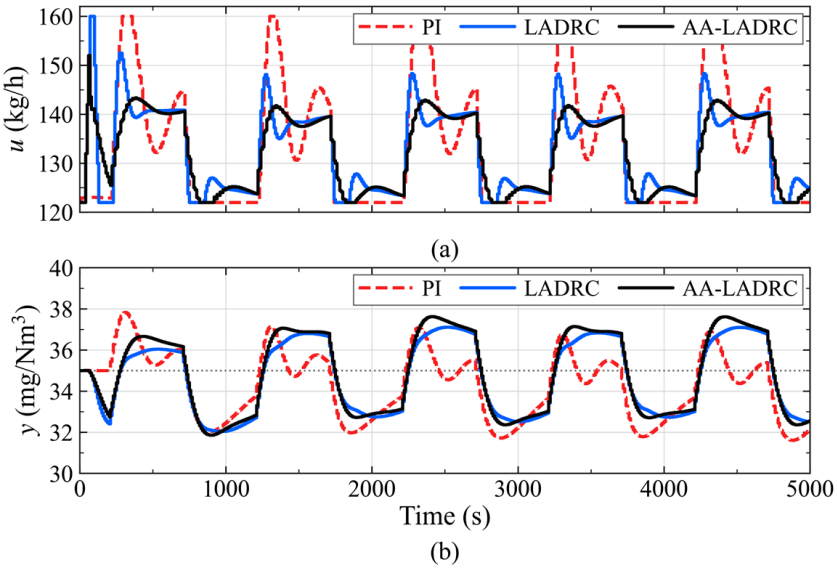


Figure 9. Dynamic responses of PI, LADRC, and AA-LADRC under synchronous ±10% variations in the two plant time constants: (**a**) ammonia-injection control signal and (**b**) outlet NOx concentration.

Table 7. Performance comparison of PI, LADRC, and AA-LADRC under synchronous ±10% variations in the two plant time constants.

Performance Index	PI	LADRC	AA-LADRC
e_{max} (mg/Nm^3)	3.39	2.96	3.13
RMSE (mg/Nm^3)	1.81	1.82	1.97
TV_u (kg/h)	518.09	417.67	293.72

6. Conclusions

For SCR denitrification systems characterized by large inertia, slow dynamics, and multiple disturbances, this study proposes an AA-ADRC framework, with AA-LADRC adopted as its linear implementation. Based on an SCR model identified from industrial operating data, a control-oriented model is established using the second-order ammonia-injection control channel and the inlet NOx disturbance channel. A finite-bandwidth anticipatory process increment derived from variations in the ammonia-injection command is introduced into the LESO measurement channel, allowing input-side dynamic information to participate earlier in state estimation and generalized-disturbance compensation. The stability analysis shows that the resulting augmented closed-loop error system is uniformly ultimately bounded under bounded disturbance-rate conditions and exponentially converges to the origin when the generalized disturbance is constant.

Simulation results under inlet NOx step disturbances, composite inlet NOx disturbances, outlet NOx measurement disturbances, and ammonia-injection disturbances show that, for the nominal industrially identified SCR model under the fixed-load conditions considered in this study, AA-LADRC exhibits notable advantages in transient recovery and ammonia-command smoothness compared with PI and conventional LADRC, while reflecting a different performance tradeoff. Under transient disturbances, AA-LADRC achieves faster error attenuation and recovery while maintaining smaller control variation. Under persistent periodic disturbances, its advantages are mainly reflected in lower output error relative to conventional LADRC and substantially smoother ammonia-injection

regulation. In the sensitivity test with synchronous ±10% variations in the two plant time constants, AA-LADRC maintains stable responses and achieves lower ammonia-command total variation than PI and LADRC.

Author Contributions: Conceptualization, J.L. and J.P.; methodology, X.L. and Z.W.; software, J.W. and Z.W.; validation, Z.W. and X.L.; formal analysis, Z.W. and X.L.; investigation, J.L. and X.L.; resources, J.L., J.P., and X.L.; data curation, J.P., Z.W., and X.L.; writing—original draft preparation, Z.W. and X.L.; writing—review and editing, Z.W., X.L., and J.P.; visualization, J.W. and Z.W.; supervision, J.L. and X.L.; project administration, J.P. and X.L.; funding acquisition, J.L. and J.W. All authors have read and agreed to the published version of the manuscript.

Funding: This research was funded by CHN Energy Investment Group, grant number GJNY-21-169.

Data Availability Statement: The original contributions presented in this study are included in this article. Further inquiries can be directed to the corresponding author.

Conflicts of Interest: The authors Jianbo Liu, Jiacheng Peng, and Jingjing Wang were employed by the company Guoneng Guohua (Beijing) Gas-Fired Co., Ltd. The authors declare that this study received funding from CHN Energy Investment Group (GJNY-21-169). The funder was not involved in the study design, collection, analysis, interpretation of data, the writing of this article, or the decision to submit it for publication.

References

1. Boningari, T.; Smirniotis, P.G. Impact of nitrogen oxides on the environment and human health: Mn-based materials for the NO_x abatement. *Curr. Opin. Chem. Eng.* **2016**, *13*, 133–141. [CrossRef]
2. Liang, Z.; Ma, X.; Lin, H.; Tang, Y. The energy consumption and environmental impacts of SCR technology in China. *Appl. Energy* **2011**, *88*, 1120–1129. [CrossRef]
3. Busca, G.; Lietti, L.; Ramis, G.; Berti, F. Chemical and mechanistic aspects of the selective catalytic reduction of NO_x by ammonia over oxide catalysts: A review. *Appl. Catal. B Environ.* **1998**, *18*, 1–36. [CrossRef]
4. Forzatti, P. Present status and perspectives in de-NO_x SCR catalysis. *Appl. Catal. A Gen.* **2001**, *222*, 221–236. [CrossRef]
5. Lai, J.K.; Wachs, I.E. A perspective on the selective catalytic reduction (SCR) of NO with NH_3 by supported V_2O_5-WO_3/TiO_2 catalysts. *ACS Catal.* **2018**, *8*, 6537–6551. [CrossRef]
6. Muzio, L.; Bogseth, S.; Himes, R.; Chien, Y.C.; Dunn-Rankin, D. Ammonium bisulfate formation and reduced load SCR operation. *Fuel* **2017**, *206*, 180–189. [CrossRef]
7. Zhao, S.; Peng, J.; Ge, R.; Yang, K.; Wu, S.; Qian, Y.; Xu, T.; Gao, J.; Chen, Y.; Sun, Z. Poisoning and regeneration of commercial V_2O_5-WO_3/TiO_2 selective catalytic reduction (SCR) catalyst in coal-fired power plants. *Process Saf. Environ. Prot.* **2022**, *168*, 971–992. [CrossRef]
8. Shah, S.; Abrol, S.; Balram, S.; Barve, J. Optimal ammonia injection for emissions control in power plants. *IFAC-Pap.* **2015**, *48*, 379–384. [CrossRef]
9. Zhang, K.; Zhao, J.; Zhu, Y. MPC case study on a selective catalytic reduction in a power plant. *J. Process Control* **2018**, *62*, 1–10. [CrossRef]
10. Gao, W.; Liu, M.; Yin, J.; Zhao, Y.; Chen, W.; Yan, J. An improved control strategy for a denitrification system using cooperative control of NH_3 injection and flue gas temperature for coal-fired power plants. *Energy* **2023**, *282*, 128759. [CrossRef]
11. Lv, Y.; Lv, X.; Fang, F.; Yang, T.; Romero, C.E. Adaptive selective catalytic reduction model development using typical operating data in coal-fired power plants. *Energy* **2020**, *192*, 116589. [CrossRef]
12. Kang, J.; Niu, Y.; Hu, B.; Li, H.; Zhou, Z. Dynamic modeling of SCR denitration systems in coal-fired power plants based on a bi-directional long short-term memory method. *Process Saf. Environ. Prot.* **2021**, *148*, 867–878. [CrossRef]
13. Lietti, L.; Nova, I.; Tronconi, E.; Forzatti, P. Transient kinetic study of the SCR-DeNO_x reaction. *Catal. Today* **1998**, *45*, 85–92. [CrossRef]
14. Nova, I.; Lietti, L.; Tronconi, E.; Forzatti, P. Dynamics of SCR reaction over a TiO_2-supported vanadia–tungsta commercial catalyst. *Catal. Today* **2000**, *60*, 73–82. [CrossRef]
15. Nova, I.; Lietti, L.; Tronconi, E.; Forzatti, P. Transient response method applied to the kinetic analysis of the DeNO_x-SCR reaction. *Chem. Eng. Sci.* **2001**, *56*, 1229–1237. [CrossRef]
16. Åström, K.J.; Hägglund, T. *Advanced PID Control*; ISA—The Instrumentation, Systems, and Automation Society: Research Triangle Park, NC, USA, 2006.

17. Zeng, L.; Li, Y.; Liao, P.; Wei, S. Adaptive disturbance rejection model predictive control and its application in a selective catalytic reduction denitrification system. *Comput. Chem. Eng.* **2020**, *140*, 106963. [CrossRef]
18. Liu, G.; Bao, W.; Zhang, W.; Shen, D.; Wang, Q.; Li, C.; Luo, K.H. An intelligent control of NH_3 injection for optimizing the NO_x/NH_3 ratio in SCR system. *J. Energy Inst.* **2019**, *92*, 1262–1269. [CrossRef]
19. Liu, G.; Zhang, Y.; Shen, D.; Yuan, B.; Li, R.; Sun, Y. Anticipatory NH_3 injection control for SCR system based on the prediction of the inlet NO_x concentration. *J. Energy Inst.* **2021**, *94*, 167–175. [CrossRef]
20. Morari, M.; Lee, J.H. Model predictive control: Past, present and future. *Comput. Chem. Eng.* **1999**, *23*, 667–682. [CrossRef]
21. Qin, S.J.; Badgwell, T.A. A survey of industrial model predictive control technology. *Control Eng. Pract.* **2003**, *11*, 733–764. [CrossRef]
22. Zheng, Y.; Jensen, A.D.; Johnsson, J.E. Deactivation of V_2O_5-WO_3-TiO_2 SCR catalyst at a biomass-fired combined heat and power plant. *Appl. Catal. B Environ.* **2005**, *60*, 253–264. [CrossRef]
23. Han, J. From PID to active disturbance rejection control. *IEEE Trans. Ind. Electron.* **2009**, *56*, 900–906. [CrossRef]
24. Gao, Z. Scaling and bandwidth-parameterization based controller tuning. In Proceedings of the 2003 American Control Conference, Denver, CO, USA, 4–6 June 2003; Volume 6, pp. 4989–4996. [CrossRef]
25. Huang, Y.; Xue, W. Active disturbance rejection control: Methodology and theoretical analysis. *ISA Trans.* **2014**, *53*, 963–976. [CrossRef]
26. Guo, B.Z.; Zhao, Z.L. On the convergence of an extended state observer for nonlinear systems with uncertainty. *Syst. Control Lett.* **2011**, *60*, 420–430. [CrossRef]
27. Herbst, G. A simulative study on active disturbance rejection control (ADRC) as a control tool for practitioners. *Electronics* **2013**, *2*, 246–279. [CrossRef]
28. Zheng, Q.; Gao, Z. Predictive active disturbance rejection control for processes with time delay. *ISA Trans.* **2014**, *53*, 873–881. [CrossRef]
29. Zhao, S.; Gao, Z. Modified active disturbance rejection control for time-delay systems. *ISA Trans.* **2014**, *53*, 882–888. [CrossRef]
30. Madoński, R.; Herman, P. Survey on methods of increasing the efficiency of extended state disturbance observers. *ISA Trans.* **2015**, *56*, 18–27. [CrossRef]
31. Chen, Z.; Hao, Y.S.; Sun, L.; Su, Z.G. Phase compensation based active disturbance rejection control for high order superheated steam temperature system. *Control Eng. Pract.* **2022**, *126*, 105200. [CrossRef]
32. Chen, J.P.; Yang, R.T. Role of WO_3 in mixed V_2O_5-WO_3/TiO_2 catalysts for selective catalytic reduction of nitric oxide with ammonia. *Appl. Catal. A Gen.* **1992**, *80*, 135–148. [CrossRef]
33. Nova, I.; Ciardelli, C.; Tronconi, E.; Chatterjee, D.; Bandl-Konrad, B. NH_3-NO/NO_2 chemistry over V-based catalysts and its role in the mechanism of the fast SCR reaction. *Catal. Today* **2006**, *114*, 3–12. [CrossRef]
34. Efstathiou, A.M.; Fliatoura, K. Selective catalytic reduction of nitric oxide with ammonia over a V_2O_5/TiO_2 catalyst: A steady-state and transient kinetic study. *Appl. Catal. B Environ.* **1995**, *6*, 35–59. [CrossRef]
35. Kamata, H.; Takahashi, K.; Odenbrand, C.U.I. Kinetics of the selective reduction of NO with NH_3 over a $V_2O_5(WO_3)/TiO_2$ commercial SCR catalyst. *J. Catal.* **1999**, *185*, 106–113. [CrossRef]
36. Rao, D.; Tan, P.; Li, Z.; Hu, C.; Cao, N.; Zhang, C.; Fang, Q.; Chen, G. Research on mechanism modeling of SCR denitrification system in coal-fired power plants. *Therm. Power Gener.* **2019**, *48*, 36–41. [CrossRef]

Disclaimer/Publisher's Note: The statements, opinions and data contained in all publications are solely those of the individual author(s) and contributor(s) and not of MDPI and/or the editor(s). MDPI and/or the editor(s) disclaim responsibility for any injury to people or property resulting from any ideas, methods, instructions or products referred to in the content.